HOP: A tool to dissect directed and causal multivariate dynamic interactions in networks of oscillatory processes

I. PIRD AND PDGC

This document describes two tools recently introduced for the analysis of high-order dynamic interactions in networks of random processes represented in both time and frequency domains. The tools are the partial information rate decomposition (PIRD) [1] and the partial decomposition of Granger causality (PDGC) [2], whose implementations are collected in the Matlab toolbox for the High-Order analysis of Random processes (HOP). The present notes are highly adherent to the supplementary material of [2], referred to as "the main paper".

First, we discuss the relation between PIRD and PDGC in the analysis of Gaussian random processes. While we refer the reader to Refs. [3], [1], [2] for a complete description of the frameworks, we focus here on the formal correspondence between the spectral redundancy-lattice decomposition performed by PIRD and PDGC. We start by replacing, in the formulation adopted in the main paper, the spectral Granger causality (GC) with the spectral mutual information rate (MIR). The MIR quantifies the information shared per unit time between the vector of source processes $X = \{X_1, \dots, X_N\}$ and the target process Y. The MIR and its spectral counterpart are denoted as $I_{X;Y}$ and $i_{X;Y}(\omega)$, evidencing a parallel with the time-domain and spectral GC $F_{X\to Y}$ and $f_{X\to Y}(\omega)$ considered in the present work.

For Gaussian processes, the spectral MIR can be expressed from the frequency-domain representation of the VAR process introduced in Eq. (3) of the main paper. Denoting by $S = \{X, Y\}$ the whole process, its power spectral density (PSD) matrix can be written as

$$\mathbf{P}_S(\omega) = \mathbf{H}_S(\omega)\mathbf{\Sigma}_U\mathbf{H}_S^*(\omega), \tag{S1}$$

where $\mathbf{H}_S(\omega)$ is the $M \times M$ transfer function matrix of the full process, $\mathbf{\Sigma}_U$ is the covariance matrix of the innovations, and $(\cdot)^*$ denotes conjugate transpose. The matrix $\mathbf{P}_S(\omega)$ can be partitioned as

$$\mathbf{P}_S(\omega) = \begin{bmatrix} \mathbf{P}_X(\omega) & \mathbf{P}_{XY}(\omega) \\ \mathbf{P}_{YX}(\omega) & P_Y(\omega) \end{bmatrix}, \tag{S2}$$

where $\mathbf{P}_X(\omega)$ is the PSD matrix of the source vector X, $P_Y(\omega)$ is the PSD of the scalar target process, and $\mathbf{P}_{XY}(\omega)$, $\mathbf{P}_{YX}(\omega)$ are the corresponding cross-spectral blocks. For jointly Gaussian processes, the spectral MIR is given by [3]

$$i_{X;Y}(\omega) = \frac{1}{2}\ln\frac{|\mathbf{P}_X(\omega)|\,P_Y(\omega)}{|\mathbf{P}_S(\omega)|}, \tag{S3}$$

where $|\cdot|$ denotes the determinant. Using the one-sided spectral representation adopted in the main paper for real-valued processes, the MIR is obtained as

$$I_{X;Y} = \frac{1}{\pi}\int_0^\pi i_{X;Y}(\omega)\,d\omega. \tag{S4}$$

For any atom $\alpha = \{\alpha_1, \dots, \alpha_J\}$ of the redundancy lattice, where each $\alpha_j \subseteq \{1 \cdots N\}$ identifies a subset of source indices, the corresponding subset of source processes is denoted by X_{α_j}. Following the notation used in the main paper for the

computation of GC, we define the restricted process $Z = \{X_{\alpha_j}, Y\} \subseteq S$. The PSD matrix of Z is

$$\mathbf{P}_Z(\omega) = \begin{bmatrix} \mathbf{P}_{X_{\alpha_j}}(\omega) & \mathbf{P}_{X_{\alpha_j}Y}(\omega) \\ \mathbf{P}_{YX_{\alpha_j}}(\omega) & P_Y(\omega) \end{bmatrix}. \tag{S5}$$

Accordingly, the spectral MIR between the subset of sources X_{α_j} and the target Y is

$$i_{X_{\alpha_j};Y}(\omega) = \frac{1}{2} \ln \frac{\left|\mathbf{P}_{X_{\alpha_j}}(\omega)\right| P_Y(\omega)}{|\mathbf{P}_Z(\omega)|}. \tag{S6}$$

This expression is the spectral-MIR counterpart of the spectral GC $f_{X_{\alpha_j} \to Y}(\omega)$ used in the PDGC formulation of the main paper.

The spectral MIR can then be decomposed, over a redundancy lattice with the same topological structure of that used to decompose the spectral GC, as follows:

$$i_{X;Y}(\omega) = \sum_{\alpha \in \mathcal{A}} i^{\delta}_{X_\alpha;Y}(\omega), \tag{S7}$$

where $i^{\delta}_{X_\alpha;Y}(\omega)$ is the spectral partial information rate associated with the atom α, and $X_\alpha = \{X_{\alpha_1}, \ldots, X_{\alpha_J}\}$ denotes the collection of source subsets composing that atom. As for PDGC, solving Eq. (S7) requires the definition of a spectral redundancy rate over the lattice. Following the spectral minimum mutual information (SMMI) criterion [1], the redundancy rate is defined as

$$i^{\cap}_{X_\alpha;Y}(\omega) = i^{\mathrm{SMMI}}_{X_\alpha;Y}(\omega) := \min_{j=1,\ldots,J} i_{X_{\alpha_j};Y}(\omega). \tag{S8}$$

The spectral redundancy rate can also be written as the sum of the spectral partial information rates of the atoms positioned at α or downwards in the lattice,

$$i^{\cap}_{X_\alpha;Y}(\omega) = \sum_{\beta \preceq \alpha} i^{\delta}_{X_\beta;Y}(\omega), \tag{S9}$$

which yields the recursive computation of the spectral partial information atoms,

$$i^{\delta}_{X_\alpha;Y}(\omega) = i^{\cap}_{X_\alpha;Y}(\omega) - \sum_{\beta \prec \alpha} i^{\delta}_{X_\beta;Y}(\omega). \tag{S10}$$

Once the spectral atoms have been obtained, they can be grouped to obtain a coarse-grained representation, in direct analogy with the coarse-grained PDGC decomposition introduced in Eq. (16) of the main paper:

$$i_{X;Y}(\omega) = i^{R}_{X;Y}(\omega) + i^{S}_{X;Y}(\omega) + \sum_{m=1}^{N} i^{U}_{X_m;Y}(\omega). \tag{S11}$$

Here, $i^{U}_{X_m;Y}(\omega)$ is the unique spectral information rate shared between the m-th source and the target, while $i^{R}_{X;Y}(\omega)$ and $i^{S}_{X;Y}(\omega)$ denote the redundant and synergistic spectral information rates associated with the whole set of sources.

Since the redundancy rate in Eq. (S8) is defined in the frequency domain, the corresponding time-domain SMMI redundancy rate is obtained by spectral integration:

$$I^{\cap}_{X_\alpha;Y} = I^{\mathrm{SMMI}}_{X_\alpha;Y} := \frac{1}{\pi} \int_0^{\pi} i^{\mathrm{SMMI}}_{X_\alpha;Y}(\omega)\, d\omega. \tag{S12}$$

This quantity can be used, in analogy with Eq. (11) of the main paper, to obtain the partial information rate associated with each atom of the lattice:

$$I^{\delta}_{X_\alpha;Y} = I^{\cap}_{X_\alpha;Y} - \sum_{\beta \prec \alpha} I^{\delta}_{X_\beta;Y}. \tag{S13}$$

Equivalently, the time-domain atoms can be obtained by direct integration of their spectral counterparts,

$$I^{\delta}_{X_\alpha;Y} = \frac{1}{\pi} \int_0^{\pi} i^{\delta}_{X_\alpha;Y}(\omega)\, d\omega. \tag{S14}$$

TABLE S1
FORMAL CORRESPONDENCE BETWEEN THE PIRD QUANTITIES INTRODUCED IN THIS SUPPLEMENTARY SECTION AND THE PDGC QUANTITIES DEFINED IN THE MAIN PAPER. THE CORRESPONDENCE IS ESTABLISHED AT THE LEVEL OF THE REDUNDANCY-LATTICE CONSTRUCTION: PIRD DECOMPOSES THE SPECTRAL MUTUAL INFORMATION RATE, WHEREAS PDGC DECOMPOSES THE SPECTRAL GRANGER-CAUSAL INFORMATION FLOW.

Role	**PIRD quantity**	**PDGC counterpart**	**Equation**
Full spectral measure	$i_{X;Y}(\omega)$	$f_{X\to Y}(\omega)$	Supp. Eq. (S3); main Eq. (15)
Subset spectral measure	$i_{X_{\alpha_j};Y}(\omega)$	$f_{X_{\alpha_j}\to Y}(\omega)$	Supp. Eq. (S6); main Eq. (9)
Fine-grained decomposition	$i_{X;Y}(\omega)=\sum_{\alpha\in\mathcal{A}} i^{\delta}_{X_\alpha;Y}(\omega)$	$f_{X\to Y}(\omega)=\sum_{\alpha\in\mathcal{A}} f^{\delta}_{X_\alpha\to Y}(\omega)$	Supp. Eq. (S7); main Eq. (15)
Spectral redundancy function	$i^{\cap}_{X_\alpha;Y}(\omega)=\min_{j=1,\dots,J} i_{X_{\alpha_j};Y}(\omega)$	$f^{\cap}_{X_\alpha\to Y}(\omega)=\min_{j=1,\dots,J} f_{X_{\alpha_j}\to Y}(\omega)$	Supp. Eq. (S8); main Eq. (13)
Lattice consistency relation	$i^{\cap}_{X_\alpha;Y}(\omega)=\sum_{\beta\preceq\alpha} i^{\delta}_{X_\beta;Y}(\omega)$	$f^{\cap}_{X_\alpha\to Y}(\omega)=\sum_{\beta\preceq\alpha} f^{\delta}_{X_\beta\to Y}(\omega)$	Supp. Eq. (S9); main Eq. (11)
Spectral atom recursion	$i^{\delta}_{X_\alpha;Y}(\omega)=i^{\cap}_{X_\alpha;Y}(\omega)-\sum_{\beta\prec\alpha} i^{\delta}_{X_\beta;Y}(\omega)$	$f^{\delta}_{X_\alpha\to Y}(\omega)=f^{\cap}_{X_\alpha\to Y}(\omega)-\sum_{\beta\prec\alpha} f^{\delta}_{X_\beta\to Y}(\omega)$	Supp. Eq. (S10); main Eq. (14)
Coarse-grained spectral decomposition	$i_{X;Y}(\omega)=i^{R}_{X;Y}(\omega)+i^{S}_{X;Y}(\omega)+\sum_{m=1}^{N} i^{U}_{X_m;Y}(\omega)$	$f_{X\to Y}(\omega)=f^{R}_{X\to Y}(\omega)+f^{S}_{X\to Y}(\omega)+\sum_{m=1}^{N} f^{U}_{X_m\to Y}(\omega)$	Supp. Eq. (S11); main Eq. (16)
Spectral-to-time integration	$I^{\delta}_{X_\alpha;Y}=\frac{1}{\pi}\int_0^{\pi} i^{\delta}_{X_\alpha;Y}(\omega)\,d\omega$	$F^{\delta}_{X_\alpha\to Y}=\frac{1}{\pi}\int_0^{\pi} f^{\delta}_{X_\alpha\to Y}(\omega)\,d\omega$	Supp. Eq. (S14); main paper after Eq. (16)
Coarse-grained time-domain decomposition	$I_{X;Y}=I^{R}_{X;Y}+I^{S}_{X;Y}+\sum_{m=1}^{N} I^{U}_{X_m;Y}$	$F_{X\to Y}=F^{R}_{X\to Y}+F^{S}_{X\to Y}+\sum_{m=1}^{N} F^{U}_{X_m\to Y}$	Supp. Eq. (S15); main Eq. (17)
Conceptual link with information transfer	$I_{X;Y}=T_{X\to Y}+T_{Y\to X}+I_{X\cdot Y}$	For Gaussian processes, $T_{X\to Y}$ is proportional to $F_{X\to Y}$ under the usual GC–TE equivalence	Supp. Eq. (S16); main Eq. (1)

Finally, whole-band integration of Eq. (S11) yields the coarse-grained PIRD in the time domain:

$$I_{X;Y}=I^{R}_{X;Y}+I^{S}_{X;Y}+\sum_{m=1}^{N} I^{U}_{X_m;Y}. \tag{S15}$$

The formal correspondence between the PIRD quantities introduced above and their PDGC counterparts introduced in the main paper is summarized in Table S1. The table emphasizes that the two frameworks share the same redundancy-lattice structure, the same recursive construction of the atoms, and the same spectral-to-time integration scheme, but differ in the elementary spectral quantity assigned to each source subset: the spectral MIR $i_{X_{\alpha_j};Y}(\omega)$ in PIRD and the spectral GC $f_{X_{\alpha_j}\to Y}(\omega)$ in PDGC.

As summarized in Table S1, the analogy between PIRD and PDGC is formal rather than conceptual. PIRD decomposes the spectral MIR $i_{X;Y}(\omega)$, which measures dynamic information sharing between sources and target, whereas PDGC decomposes the spectral GC $f_{X\to Y}(\omega)$, which measures the directed predictive influences from the sources to the target. The two quantities are nevertheless related because the MIR between two processes can be written as the sum of the transfer entropy from X to Y, the transfer entropy from Y to X, and the instantaneous information shared by the two processes [4]:

$$I_{X;Y}=T_{X\to Y}+T_{Y\to X}+I_{X\cdot Y}. \tag{S16}$$

For Gaussian processes, transfer entropy is equal to half the Geweke's GC expressed in logarithmic form [5]. Under a strictly causal model assumption, $I_{X\cdot Y}=0$, and the MIR reduces to the sum of the two transfer-entropy terms, which are directly related to the GC from X to Y and from Y to X. It is important to stress that, in the general case, PIRD and PDGC should not be interpreted as equivalent decompositions, because PIRD includes bidirectional and instantaneous information-sharing effects, whereas PDGC isolates the directed predictive contribution from the sources to the target.

II. IMPLEMENTATION OF PDGC

This section describes the practical realization of the framework for computing the PDGC measures in networks of Gaussian random processes. The presentation refers to the methodological formulation introduced in the main paper (Sect. II.B,C) and to the schematic workflow reported in Fig. S1, and includes description of the codes implementing in practice the various measures; the latter provided in the HOP MATLAB Toolbox (High-Order analysis of random Processes, www.lucafaes.net/hop.html, https://github.com/YuriAntonacci/HOP).

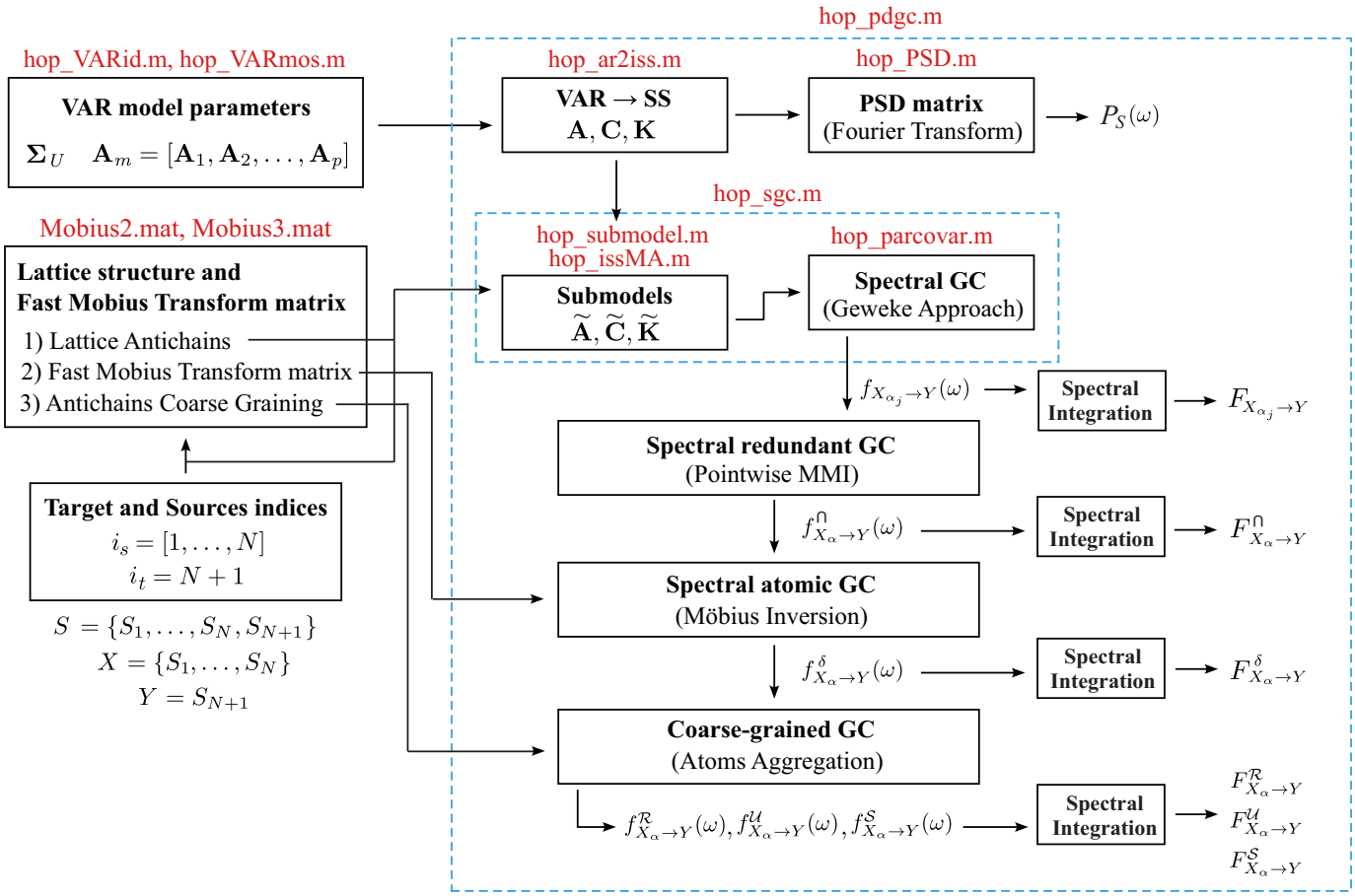

Fig. S1. Schematic description of the algorithmic implementation of the framework for PDGC computation. Blocks represent the operations applied to processes/spectral functions for deriving the various measures. The functions of the HOP MATLAB Toolbox implemented by the procedure are reported close to the various blocks.

The procedure starts from a full multivariate VAR model and derives the innovations-form state-space quantities required to compute the spectral measures entering the redundancy lattice. The computation of PDGC shares with PIRD the same computational structure up to the construction of the restricted state-space models associated with each source subset and the target; they differ, however, in the frequency-domain quantity assigned to the lattice: PDGC decomposes the full spectral GC from the sources to the target, whereas PIRD decomposes the multivariate spectral MIR between sources and target. In addition, the PIRD implementation also provides the frequency-domain decomposition of the MIR into two directional transfer entropy (TE) terms and an instantaneous information term, following the OIR framework [6]. This TE-based output is related to GC for Gaussian processes, but it does not generally coincide with the Geweke spectral GC used in PDGC when instantaneous effects are present, as discussed below.

A. VAR and SS model identification

Let $S_n = [S_{1,n}, \ldots, S_{M,n}]^\top$ be a real-valued, zero-mean, stationary Gaussian process, partitioned into a set of N source processes $X = \{X_1, \ldots, X_N\}$ and a scalar target process Y, with $M = N + 1$. The starting point is an $M \times N_s$ data matrix containing the M time series of length N_s, interpreted as one realization of the multivariate process S. The process is modeled through the VAR representation introduced in Eq. (3) of the main paper,

$$S_n = \sum_{k=1}^{p} \mathbf{A}_k S_{n-k} + U_n, \tag{S17}$$

where $\mathbf{A}_k \in \mathbb{R}^{M \times M}$ are the VAR coefficient matrices, p is the model order, and U_n is a white Gaussian innovation process with covariance matrix $\mathbf{\Sigma}_U \in \mathbb{R}^{M \times M}$. In practical applications, the model order p is optimized using the Akaike Information

Criterion (AIC) [7] or the Bayesian Information Criterion (BIC) [8]; these criteria are implemented in the HOP toolbox through the function `hop_VARmos.m`. Once the order has been fixed, the VAR model is identified by classical least-squares estimation [9] (function `hop_VARid.m`), yielding estimates of the coefficient matrices $[\mathbf{A}_1, \ldots, \mathbf{A}_p]$ and of the innovation covariance matrix $\mathbf{\Sigma}_U$.

The identified VAR model is then converted into the equivalent innovations-form state-space representation (Eq. (18) of the main paper),

$$S_n = \mathbf{C}\bar{S}_n + U_n, \tag{S18a}$$

$$\bar{S}_{n+1} = \mathbf{A}\bar{S}_n + \mathbf{K}U_n, \tag{S18b}$$

where $\bar{S}_n = [S_{n-1}^\top \cdots S_{n-p}^\top]^\top \in \mathbb{R}^{pM}$ is the state vector. The matrices of the innovations-form state-space representation are

$$\mathbf{C} = \begin{bmatrix} \mathbf{A}_1 & \mathbf{A}_2 & \cdots & \mathbf{A}_p \end{bmatrix} \in \mathbb{R}^{M \times pM}, \tag{S19}$$

$$\mathbf{A} = \begin{bmatrix} \mathbf{A}_1 & \mathbf{A}_2 & \cdots & \mathbf{A}_{p-1} & \mathbf{A}_p \\ \mathbf{I}_M & \mathbf{0}_M & \cdots & \mathbf{0}_M & \mathbf{0}_M \\ \mathbf{0}_M & \mathbf{I}_M & \cdots & \mathbf{0}_M & \mathbf{0}_M \\ \vdots & \vdots & \ddots & \vdots & \vdots \\ \mathbf{0}_M & \mathbf{0}_M & \cdots & \mathbf{I}_M & \mathbf{0}_M \end{bmatrix} \in \mathbb{R}^{pM \times pM}, \tag{S20}$$

and

$$\mathbf{K} = \begin{bmatrix} \mathbf{I}_M \\ \mathbf{0}_{M(p-1)\times M} \end{bmatrix} \in \mathbb{R}^{pM \times M}, \tag{S21}$$

where $\mathbf{I}$ and $\mathbf{0}$ denote identity and null matrices of suitable dimensions. In the HOP toolbox, the conversion from the VAR to the SS parameters formalized in Eqs. (S20-S21) is performed by the function `hop_ar2iss.m`.

Then, for each source subset X_{α_j} entering the redundancy lattice, we consider the restricted process $Z = \{X_{\alpha_j}, Y\} \subseteq S$, obtained by retaining only the variables of the selected source subset and the target. If X_{α_j} contains N_j source processes, this restricted process is written as $Z_n = [X_{\alpha_j,n}^\top \; Y_n]^\top \in \mathbb{R}^K$, with $K = N_j + 1$. Its state-space representation is derived from the full model (S18) by selecting, in the observation equation (S18a), the rows associated with the variables included in Z. This row-selection step defines the reduced observation matrix $\tilde{\mathbf{C}}$; however, the resulting model is not, in general, in innovations form. Therefore, the restricted model is converted back into an innovations-form state-space representation by solving a discrete algebraic Riccati equation [10], which provides the reduced Kalman gain $\tilde{\mathbf{K}}$ and the reduced innovation covariance matrix $\mathbf{\Sigma}_W$. The restricted innovations-form model can be written as

$$Z_n = \tilde{\mathbf{C}}\bar{S}_n + W_n, \tag{S22a}$$

$$\bar{S}_{n+1} = \tilde{\mathbf{A}}\bar{S}_n + \tilde{\mathbf{K}}W_n, \tag{S22b}$$

where W_n is the innovation process of the restricted model, with covariance matrix $\mathbf{\Sigma}_W \in \mathbb{R}^{K\times K}$. Here, $\tilde{\mathbf{A}} = \mathbf{A}$, while $\tilde{\mathbf{C}}$ contains the rows of $\mathbf{C}$ associated with the variables included in Z; conversely, $\tilde{\mathbf{K}}$ and $\mathbf{\Sigma}_W$ are obtained from the solution to the Riccati equation. In the HOP toolbox implementation, this submodel identification step is performed by `hop_submodel.m`.

B. Spectral computation

In the frequency domain, the $K \times K$ transfer function matrix of the restricted innovations-form state-space model is obtained as [10], [6]

$$\mathbf{H}(\omega) = \mathbf{I}_K + \tilde{\mathbf{C}}\left(\mathbf{I}_{Mp} - \tilde{\mathbf{A}}e^{-j\omega}\right)^{-1}\tilde{\mathbf{K}}e^{-j\omega}, \tag{S23}$$

where $\mathbf{I}_K$ and $\mathbf{I}_{Mp}$ are identity matrices of dimension K and Mp, respectively. The corresponding PSD matrix of Z is then computed as

$$\mathbf{P}_Z(\omega) = \mathbf{H}(\omega)\mathbf{\Sigma}_W\mathbf{H}^*(\omega), \tag{S24}$$

where $(\cdot)^*$ denotes conjugate transpose. Starting from the restricted spectral representation in Eq. (S24), the PDGC computation assigns to each source subset X_{α_j} the spectral GC from X_{α_j} to Y; in the HOP toolbox, this step is performed by the function `hop_sgc.m`. To derive the corresponding spectral GC, the restricted process is partitioned as $Z_1 = X_{\alpha_j}$ and $Z_2 = Y$, so that

$$\mathbf{H}(\omega) = \begin{bmatrix} \mathbf{H}_{11}(\omega) & \mathbf{H}_{12}(\omega) \\ \mathbf{H}_{21}(\omega) & H_{22}(\omega) \end{bmatrix}, \qquad \mathbf{\Sigma}_W = \begin{bmatrix} \mathbf{\Sigma}_1 & \mathbf{\Sigma}_{12} \\ \mathbf{\Sigma}_{21} & \sigma_2^2 \end{bmatrix}. \tag{S25}$$

Here, $\mathbf{\Sigma}_1$ is the innovation covariance of the driver block, σ_2^2 is the innovation variance of the scalar target, and $\mathbf{\Sigma}_{12}$ and $\mathbf{\Sigma}_{21}$ encode possible instantaneous correlations between driver and target innovations. Thus, in the restricted ISS representation, zero-lag dependencies are not encoded in the transfer function alone, but enter the spectral matrix through the off-diagonal blocks of $\mathbf{\Sigma}_W$. To remove zero-lag dependencies from the spectral factorization, the frequency-domain formulation of the main paper introduces the transformed innovations

$$\tilde{W}_{1,n} = W_{1,n} - \mathbf{\Sigma}_{12}(\sigma_2^2)^{-1} W_{2,n}, \qquad \tilde{W}_{2,n} = W_{2,n}. \tag{S26}$$

This operation makes block diagonal the covariance matrix of the transformed innovations $\tilde{W}_n = [\tilde{W}_{1,n}^\top \, W_{2,n}]^\top$, i.e.

$$\mathbf{\Sigma}_{\tilde{W}} = \begin{bmatrix} \tilde{\mathbf{\Sigma}}_1 & \mathbf{0} \\ \mathbf{0} & \sigma_2^2 \end{bmatrix}, \qquad \tilde{\mathbf{\Sigma}}_1 = \mathbf{\Sigma}_1 - \mathbf{\Sigma}_{12}(\sigma_2^2)^{-1}\mathbf{\Sigma}_{21}. \tag{S27}$$

Equivalently, $\tilde{\mathbf{\Sigma}}_1$ is the partial covariance of the driver innovations after removing the component linearly associated with the target innovation. In the HOP toolbox, it is computed by the function `hop_parcovar.m`, used inside `hop_sgc.m`. With this representation, the PSD of the target can be written simply as the sum of two contributions:

$$P_Y(\omega) = \tilde{\mathbf{H}}_{21}(\omega)\tilde{\mathbf{\Sigma}}_1\tilde{\mathbf{H}}_{21}^*(\omega) + \sigma_2^2|\tilde{H}_{22}(\omega)|^2, \tag{S28}$$

which leads to the frequency-domain GC formulation provided by Geweke [11] (Eq. (9) of the main paper):

$$f_{X_{\alpha_j}\to Y}(\omega) = \ln \frac{P_Y(\omega)}{\sigma_2^2|\tilde{H}_{22}(\omega)|^2}. \tag{S29}$$

Notably, in the state-space implementation, the transfer function $\tilde{\mathbf{H}}(\omega)$ appearing in the transformed frequency-domain derivation is not reconstructed explicitly. Instead, the spectral GC is evaluated using the transfer function $\mathbf{H}(\omega)$ of the restricted ISS model. Although the two transfer functions differ in the column associated with the target innovation, they share the block mapping driver innovations to the target:

$$\mathbf{H}_{21}(\omega) = \tilde{\mathbf{H}}_{21}(\omega). \tag{S30}$$

Therefore, using Eq. (S28) and exploiting the equivalence of Eq. (S30), the denominator of Eq. (S29) can therefore be rewritten as

$$\sigma_2^2|\tilde{H}_{22}(\omega)|^2 = P_Y(\omega) - \mathbf{H}_{21}(\omega)\tilde{\mathbf{\Sigma}}_1\mathbf{H}_{21}^*(\omega), \tag{S31}$$

which yields the state-space form of the spectral GC used for PDGC (Eq. (21) of the main paper):

$$f_{X_{\alpha_j}\to Y}(\omega) = \ln \frac{P_Y(\omega)}{P_Y(\omega) - \mathbf{H}_{21}(\omega)\tilde{\mathbf{\Sigma}}_1\mathbf{H}_{21}^*(\omega)}. \tag{S32}$$

C. Comparison between spectral GC and spectral TE

The restricted ISS model formulated in (S22) is also used in the PIRD implementation to compute the spectral MIR and its causal decomposition according to the PIRD framework [1]. For the pair (X_{α_j}, Y), the spectral MIR can be written as

$$i_{X_{\alpha_j};Y}(\omega) = t_{X_{\alpha_j}\to Y}(\omega) + t_{Y\to X_{\alpha_j}}(\omega) + i_{X_{\alpha_j}\cdot Y}(\omega), \tag{S33}$$

where the first two terms quantify the two directional transfer entropy (TE) contributions, and the last term is the instantaneous information shared by X_{α_j} and Y. This decomposition is implemented in `hop_mir.m`. With the same partition adopted above,

the contribution from X_{α_j} to Y is given by the spectral TE

$$t_{X_{\alpha_j}\to Y}(\omega) = \frac{1}{2}\ln\frac{P_Y(\omega)}{\sigma_2^2\left|H_{22}(\omega)\right|^2}, \tag{S34}$$

where $H_{22}(\omega)$ propagates the target innovation $W_{2,n}$ to Y in the restricted ISS model. To compare Eq. (S34) with the PDGC, the PSD of the target obtained from Eq. (S24) can be expanded using the partition in Eq. (S25), in which the innovation covariance is not block-diagonal:

$$P_Y(\omega) = \mathbf{H}_{21}(\omega)\mathbf{\Sigma}_1\mathbf{H}_{21}^*(\omega) + \mathbf{H}_{21}(\omega)\mathbf{\Sigma}_{12}H_{22}^*(\omega) + H_{22}(\omega)\mathbf{\Sigma}_{21}\mathbf{H}_{21}^*(\omega) + \sigma_2^2\left|H_{22}(\omega)\right|^2. \tag{S35}$$

Therefore, Eq. (S34) is equivalently

$$t_{X_{\alpha_j}\to Y}(\omega) = \frac{1}{2}\ln\frac{P_Y(\omega)}{P_Y(\omega) - \left[\mathbf{H}_{21}(\omega)\mathbf{\Sigma}_1\mathbf{H}_{21}^*(\omega) + \mathbf{H}_{21}(\omega)\mathbf{\Sigma}_{12}H_{22}^*(\omega) + H_{22}(\omega)\mathbf{\Sigma}_{21}\mathbf{H}_{21}^*(\omega)\right]}. \tag{S36}$$

Equations (S36,S34) and (S32,S29) both quatify spectral GC as a logarithmic ratio between the PSD of the target Y and the part of such PSD that is ascribed to internal (non-causal) dynamics in the target itself. However, they differ in the way the non-causal spectral contribution to $P_Y(\omega)$ is computed: the spectral GC (S34) used in this paper is the Geweke measure [11] that expresses $P_Y(\omega)$ through Eq. (S28), thus effectively isolating the internal and causal contributions to the target spectrum; the spectral TE (S34) used in [6] expresses $P_Y(\omega)$ through Eq. (S35), which includes two terms that mix the autonomous and causal contributions to the target spectrum (represented respectively by the TFs $H_{22}(\omega)$ and $\mathbf{H}_{21}(\omega)$). As a consequence, the Geweke approach used here should be preferred to estimate spectral causality when instantaneous effects are present, because of its ability to disentangle autonomous and causal contributions to the target spectrum. On the other hand, the approach used in [6], although including in the GC measure some of the internal target dynamics, should be preferred when an overall description of the process is sought (e.g., when it is required to compute spectral GCs over the two causal directions from a single model representation to assess the spectral MIR). It is worth noting that this distinctin holds only in the presence of instantaneous effects among the observed processes, because the two quantities coincide, apart from the 0.5 factor relating TE and GC for Gaussian processes, when $\mathbf{\Sigma}_{12} = \mathbf{\Sigma}_{21} = \mathbf{0}$; in such a case we have $\tilde{\mathbf{\Sigma}}_1 = \mathbf{\Sigma}_1$ and

$$f_{X_{\alpha_j}\to Y}(\omega) = 2\,t_{X_{\alpha_j}\to Y}(\omega). \tag{S37}$$

In the HOP toolbox, the Geweke spectral GC (S34) is computed by the function `hop_sgc.m`, while th decomposition of the spectral MIR (S33) which evidences the spectral TE (S34) is performed by the function `hop_mir.m`.

D. Coarse graining

This section formalizes the coarse-graining rules used to aggregate, when $N > 2$ source processes are considered, the PID atoms into meaningful contributions expressing the unique, redundant and synergistic GC components of the full GC computed in the frequency or time domains (Eqs. (16) and (17) of the main paper). The definitions follow those introduced by Rosas et al. [12] (k^{th}- order synergistic, redundant and unique information), considering the first-order definitions ($k = 1$) and adapting them to the decomposition of the full GC; here the rules are reported with reference with the time-domain full GC $F_{X\to Y}$.

First, the synergistic GC from N source processes $\{X_1, \ldots, X_N\}$ towards a target process Y is defined as

$$F_{X\to Y}^{\mathcal{S}} = \sum_{\alpha\in\mathcal{A}_{\mathcal{S}}} F_{X_\alpha\to Y}^{\delta}, \tag{S38}$$

where $\mathcal{A}_{\mathcal{S}} = \{\{\alpha_1, \ldots, \alpha_J\} \in \mathcal{A} : |\alpha_j| > 1, \forall j = 1, \ldots, J\}$. Intuitively, $F_{X\to Y}^{\mathcal{S}}$ collects all Granger-causal effects provided by the whole set of driver processes but not by any individual driver considered separately from the others. For example, in the presence of $N = 3$ drivers, the atoms providing synergistic information according to this rule are aggregated according to (S38) as shown in Fig. 1 of the main paper (belonging to the blue shaded area).

Similarly, the unique GC from X_i to Y ($i \in [1, \ldots, N]$) is defined as

$$F_{X_i\to Y}^{\mathcal{U}} = \sum_{\alpha\in\mathcal{A}_{\mathcal{U}}(\beta)} F_{X_\alpha\to Y}^{\delta}, \tag{S39}$$

where $\mathcal{A}_{\mathcal{U}}(\beta) = \{\alpha \in \mathcal{A} : \{i\} \in \alpha, \forall \gamma \in \alpha \backslash \{i\}, |\gamma| > 1\}$. This set includes all the atoms where $\{i\}$ is the only source with cardinality 1 (single source). Intuitively, $F^{\mathcal{U}}_{X_i \to Y}$ collects the Granger-causal effects provided to the target by the i^{th} driver but not by any other driver considered on its own. Notably, the set of unique GC atoms does not include just $F^{\delta}_{X_i \to Y}$; the two atoms aggregated when $N = 3$ sources are present are shown in Fig. 1 of the main paper (pink area for $F^{\delta}_{X_1 \to Y}$, green area for $F^{\delta}_{X_2 \to Y}$, and orange area for $F^{\delta}_{X_3 \to Y}$).

Finally, the redundant GC from $\{X_1, \ldots, X_n\}$ to Y is defined as

$$F^{\mathcal{R}}_{X \to Y} = \sum_{\alpha \in \mathcal{A}_{\mathcal{R}}} F^{\delta}_{X_\alpha \to Y}, \tag{S40}$$

where $\mathcal{A}_{\mathcal{R}} = \{\{\alpha_1, \ldots, \alpha_J\} \in \mathcal{A} : \exists i \neq j, |\alpha_i|, |\alpha_j| = 1\}$. Intuitively, $F^{\mathcal{R}}_{X \to Y}$ collects all Granger-causal effects that are brought identically to the target by at least two different drivers considered individually. For instance, in the case of $N = 3$ drivers the atoms providing redundant information are aggregated according to (S40) as indicated by the red shaded area in Fig. 1 of the main paper.

Importantly, while the aggregation rules defined above are effective when $N \geq 3$ drivers are considered, they recover the standard meaning for redundancy, synergy and unique information transfer when $N = 2$, i.e. $F^{\mathcal{R}}_{X \to Y} = F^{\delta}_{X_{\{1\}\{2\}} \to Y}$, $F^{\mathcal{S}}_{X \to Y} = F^{\delta}_{X_{\{12\}} \to Y}$, and $F^{\mathcal{U}}_{X_i \to Y} = F^{\delta}_{X_{\{i\}} \to Y}$ $(i = 1, 2)$.

III. Simulation studies

The two simulations were designed to assess complementary aspects of the proposed decomposition framework. Simulation 1, described in the main paper, considers a four-variate VAR process with three source processes and one target, and aims to test whether the coarse-grained PDGC can recover frequency-specific unique, redundant, and synergistic causal contributions in a system where direct and indirect causal pathways coexist. Simulation 2, described here in detail, considers a trivariate VAR process analyzed under the three possible target-source configurations, obtained by selecting each scalar process S_i, one at a time, as the target Y and by treating the other two processes as the source set X. This simulation is designed to compare the spectral PIRD decomposition of the MIR shared between X and Y with the spectral PDGC decomposition of the GC from X to Y, and to show that the two descriptions agree when the information shared between sources and target is mainly supported by causal effects directed from X to Y, whereas they differ when the statistical dependence between X and Y is shaped by indirect pathways or by causal effects that are not directed toward the selected target.

In both simulations, the theoretical measures were evaluated directly from the parameters of the corresponding VAR model. Specifically, the coefficient matrices and the innovation covariance matrix were used to derive the frequency-domain representation of the process and, from it, the associated power spectral density matrix $\mathbf{P}_S(\omega)$. For the PIRD analysis, the PSD matrix of the full process $S = \{X, Y\}$ was used to compute the spectral MIR $i_{X;Y}(\omega)$, together with the spectral MIR terms $i_{X_{\alpha_j};Y}(\omega)$ associated with the source subsets entering the atoms of the redundancy lattice. The spectral redundancy rate was then defined according to the SMMI criterion, by taking at each frequency the minimum of the spectral MIR values associated with the source subsets composing each atom [1]. The spectral PI-rate atoms $i^{\delta}_{X_\alpha;Y}(\omega)$ were subsequently obtained via Möbius inversion and then aggregated, according to the coarse-graining rules of the PIRD framework, to yield the corresponding unique, redundant, and synergistic spectral information-rate components.

For the PDGC analysis, the same target-source configurations and the same redundancy-lattice structure were used, but the spectral MIR terms were replaced by spectral GC terms. Specifically, for each source subset X_{α_j}, the restricted process $Z = X_{\alpha_j}, Y \subseteq S$ was considered to compute the spectral GC $f_{X_{\alpha_j} \to Y}(\omega)$. The spectral redundant GC was then obtained using the MMI criterion, by taking, at each frequency, the minimum of the spectral GC values from the source subsets composing the atom to the target. The spectral GC atoms $f^{\delta}_{X_\alpha \to Y}(\omega)$ were computed through the same lattice recursion and then aggregated according to the coarse-graining rules described in the main paper, yielding the unique, redundant, and synergistic spectral GC components.

A. Simulation 1

To study the behavior of the PDGC, we designed a four-variate Gaussian process configured to reproduce the coexistence of redundant and synergistic causal interactions from the source processes $X = [S_1, S_2, S_3]$ towards the target process $Y = S_4$. The system consists of four Gaussian systems whose dynamics are described by a VAR model of order 2, defined as follows:

$$S_{1,n} = a_{11,1}S_{1,n-1} + a_{11,2}S_{1,n-2} + U_{1,n}, \tag{S41a}$$

$$S_{2,n} = a_{21,1}S_{1,n-1} + a_{22,1}S_{2,n-1} + a_{22,2}S_{2,n-2} + U_{2,n}, \tag{S41b}$$

$$S_{3,n} = a_{33,1}S_{3,n-1} + a_{33,2}S_{3,n-2} + U_{3,n}, \tag{S41c}$$

$$S_{4,n} = a_{42,1}S_{2,n-1} + a_{43,1}S_{3,n-1} + U_{4,n}, \tag{S41d}$$

where $U_n = [U_{1,n}, \dots, U_{4,n}]^\top$ is a vector of zero-mean mutually uncorrelated white Gaussian noise processes, with variances set to $\sigma^2_{U_1} = 2$, $\sigma^2_{U_2} = 1.5$, $\sigma^2_{U_3} = 0.75$, and $\sigma^2_{U_4} = 1$. The self-dependency coefficients $a_{ii,k}$, with $i = 1, 2, 3$ and $k = 1, 2$, were set so as to generate autonomous oscillations in S_1, S_2, and S_3. Specifically, for each process S_i, one pair of complex-conjugate poles is placed in the complex plane with modulus ρ_i and phase $\phi_i = 2\pi f_i/f_s$, where $f_s = 1$ Hz. We set $\rho_1 = 0.94$, $\rho_2 = \rho_3 = 0.9$, and normalized frequencies $f_1/f_s = 0.1$, $f_2/f_s = 0.3$, and $f_3/f_s = 0.4$. Finally, the coefficients controlling the directed couplings $S_1 \to S_2$, $S_2 \to S_4$, and $S_3 \to S_4$ were set to $a_{21,1} = a_{42,1} = a_{43,1} = 1$. The simulated network is designed so that S_2 and S_3 exert direct causal influences on the target, whereas S_1 affects the target only indirectly through its influence on S_2. This configuration is used to evaluate whether the coarse-grained PDGC decomposition can separate frequency-specific unique, redundant, and synergistic causal contributions according to the underlying interaction structure. Since in this simulation $N = 3$ source processes are considered, the GC atoms were grouped according to the coarse-graining rules described in in Sect S.II.d, yielding the three unique spectral GC contributions $f^U_{X_1\to Y}(\omega)$, $f^U_{X_2\to Y}(\omega)$, and $f^U_{X_3\to Y}(\omega)$, together with the redundant spectral GC $f^R_{X\to Y}(\omega)$ and the synergistic spectral GC $f^S_{X\to Y}(\omega)$. This simulation is implemented by the script `SCRIPT_Simu1.m` of the HOP Matlab toolbox and the results are presented in the main paper (Sect. III).

Additionally, to assess the performance of the estimation procedure in a realistic setting and to relate the simulations to the analysis of short-term cardiovascular and cerebrovascular variability presented in the main paper, 100 realizations of the process S were generated, each with length $N_s = 250$ time steps. Firstly, a parameter $c \in [0, 1]$ was introduced and varied to modulate the relative strength of two directed couplings: the coefficient from S_3 to S_4 was set to $a_{43,1} = 1 - c$, whereas the coefficient from S_1 to S_2 was set to $a_{21,1} = c$, while p was fixed to the true model order. Then, the coupling parameter was fixed at $c = 0.5$, and the model order used for VAR identification was varied from $p = 1$ to $p = 8$ in order to assess the effect of model-order misspecification on the estimated PDGC components. In both analyses, for each realization and for each value of the varying parameter, the VAR parameters $\widehat{\mathbf{A}}$ and $\widehat{\mathbf{\Sigma}}_U$ were estimated from the simulated time series and used to compute the coarse-grained PDGC components. The results are presented in Fig. S2, where solid lines denote the theoretical values of the relevant measures, whereas dashed lines indicate the estimates averaged across the 100 realizations; the shaded areas represent the corresponding standard deviations, reported as a function of the coupling parameter c (panel *a*) and of the model order p (panel *b*). The first analysis, reported in Fig. S2*a*, shows that increasing the coupling parameter c drives the system from a predominantly synergistic to a predominantly redundant causal interaction structure. When $c = 0$, the process S_1 is disconnected from the remaining three processes, while S_2 and S_3 both send direct causal information to the target S_4. In this configuration, the network realizes a common-child structure, which is associated with a prevalent synergistic contribution. Conversely, when $c = 1$, the link from S_3 to the target is removed and the system reduces to the chain structure $S_1 \to S_2 \to S_4$, for which the redundant component becomes dominant and the synergistic contribution is negligible. This behavior is consistent with previous analyses based on the OIR framework, where common-child configurations were shown to favor synergistic contributions, whereas chain-like and common-driver structures were mainly associated with redundancy [13]. The same transition is reflected in the unique components. As c increases, the unique contribution of S_3 progressively decreases, consistently with the weakening of the direct link $S_3 \to S_4$, whereas the unique contribution of S_2 increases as the interaction structure becomes dominated by the pathway involving S_2 and the target. By contrast, the unique contribution of S_1 remains close to zero across the whole range of c, because S_1 does not send a direct causal influence to the target but affects

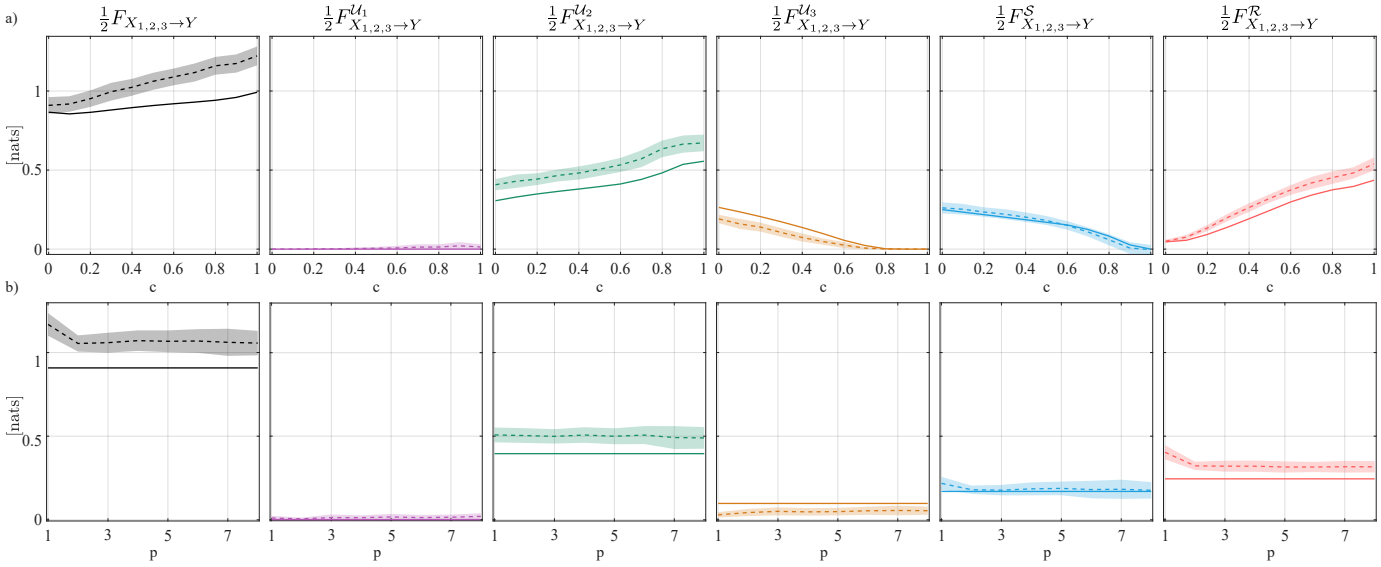

Fig. S2. PDGC analysis of the simulated VAR system in Eq. (S41), composed of three driver processes and one target process. Solid lines denote the theoretical profiles, dashed lines denote the time-domain estimates averaged across finite-length realizations after the coarse-graining procedure, and shaded areas represent the corresponding standard deviations. Panel (a) shows the results obtained by varying the coupling parameter c, while keeping the model order fixed to the true order of the simulated VAR process. Panel (b) shows the results obtained for fixed coupling strength $c = 0.5$, while varying the model order used for identification from $p = 1$ to $p = 8$ to assess the effect of model-order misspecification.

S_4 only indirectly through S_2. Accordingly, its causal contribution is mainly captured as redundant with that of S_2 rather than as a unique component, in agreement with the MMI-based redundancy criterion [3], [1]. Clearly, all these variations are not reproduced in Fig. S2*b* where the coupling parameter is set to $c = 0.5$, yielding intermediate redundancy and synergy values.

Regarding the estimation procedure, panel *a* shows that the estimated values closely follow the theoretical trends across the whole range of variation of the coupling parameter c. This supports the reliability of the estimation approach for finite-length realizations and agrees with the results reported in the main paper, where accurate estimates were obtained for time series of comparable length, namely $N_s = 250$. Results confirm also the bias of the estimates, especially for the redundant and unique GCs, showing that is dependenton the coupling parameters for some measures. In spite of such bias, the estimated PDGC components were able to follow their expected trends, documenting the ability of the estimation method to reflect changes in the mechanistic structure of the analyzed process. Moreover, panel *b* shows that the theoretical trends are preserved even when the model order used for identification is larger than the true order of the simulated process, indicating that moderate overestimation of the VAR order does not substantially alter the recovered coarse-grained PDGC components. The largest bias is instead observed when the model order is underestimated, especially for $p = 1$. This behavior is expected because the simulated dynamics contain oscillatory components generated by complex-conjugate poles of the VAR transfer function; since at least one pair of complex-conjugate poles is required to reproduce one oscillatory component, a first-order VAR model cannot provide a sufficiently rich spectral representation of the process. As a consequence, the transfer function estimated with $p = 1$ fails to capture the oscillatory structure of the data, leading to more biased estimates of the PDGC components.

B. Simulation 2

Here we investigate the frequency-domain behavior of the PIRD measure obtained by decomposing the MIR between a target process Y and two source processes X_1, X_2, and compare it with the corresponding PDGC decomposition of the spectral GC from the two sources to the target. With this aim, we use a three-variate VAR process S_1, S_2, S_3, whose dynamics and

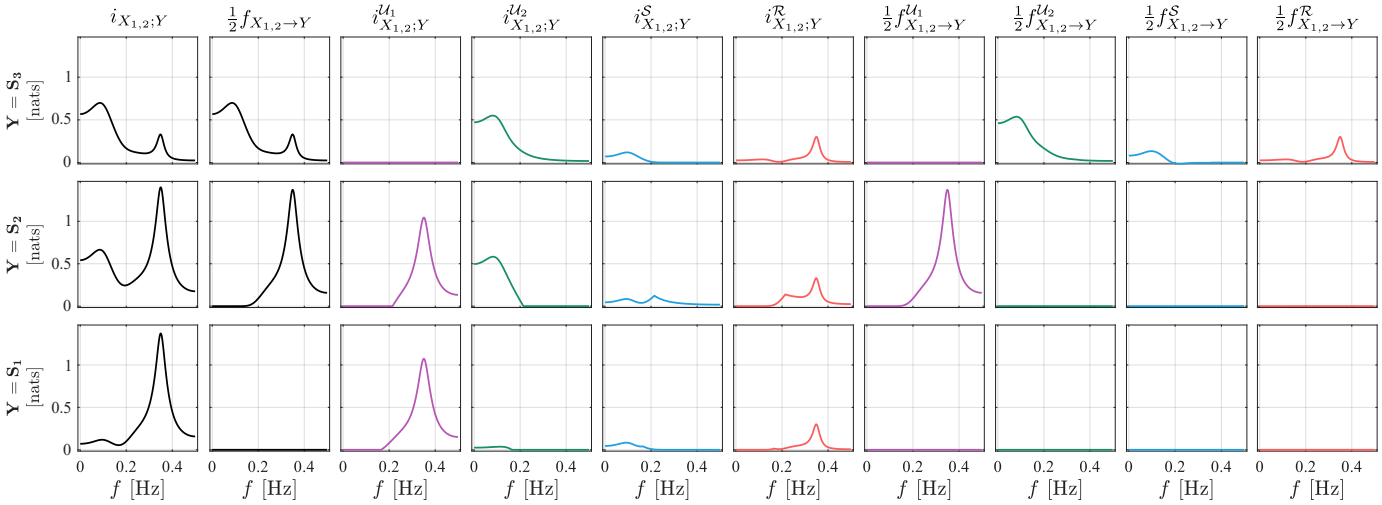

Fig. S3. PDCG and PIRD comparison in the simulated VAR system in Eq. (S42), composed of two driver processes and one target process. Solid lines denote the theoretical profiles obtained in three different configurations where is varied the processes to be considered as a target performed in the frequency domain and according to the coarse-graining procedure.

interactions are defined by the trivariate VAR model introduced in [6]:

$$S_{1,n} = \sum_{k=1}^{4} a_{11,k} S_{1,n-k} + U_{1,n}, \tag{S42a}$$

$$S_{2,n} = \sum_{k=1}^{q+1} a_{21,k} S_{1,n-k} + a_{22,1} S_{2,n-1} + a_{22,2} S_{2,n-2} + U_{2,n}, \tag{S42b}$$

$$S_{3,n} = \sum_{k=1}^{q+1} a_{31,k} S_{1,n-k} + a_{32,1} S_{2,n-1} + U_{3,n}. \tag{S42c}$$

In Eq. (S42), U_1, U_2, and U_3 are zero-mean, mutually uncorrelated white Gaussian noise processes, with variances set to $\sigma^2_{U_1} = 2$, $\sigma^2_{U_2} = 0.5$, and $\sigma^2_{U_3} = 2$. Self-dependencies are introduced for the processes S_1 and S_2 through the coefficients $a_{ii,k}$, with $i = 1, 2$, which are assigned by placing complex-conjugate poles in the complex plane. For S_1, two pairs of complex-conjugate poles are placed with moduli $\rho_{11} = 0.7$ and $\rho_{12} = 0.9$, and phases $\phi_{11} = 2\pi f_{11}/f_s$ and $\phi_{12} = 2\pi f_{12}/f_s$, with $f_{11}/f_s = 0.1$ and $f_{12}/f_s = 0.35$. This generates autonomous stochastic oscillations with central frequency 0.1 Hz and 0.35 Hz. For S_2, one pair of complex-conjugate poles is placed with modulus $\rho_2 = 0.7$ and phase $\phi_2 = 2\pi f_2/f_s$, with $f_2/f_s = 0.1$, generating an autonomous oscillation at approximately 0.1 Hz. As in Simulation 1, frequencies are expressed in Hz by assuming a sampling frequency $f_s = 1$ Hz. The coefficients determining the causal dependencies between pairs of processes are set as follows. The coefficients $a_{21,k}$ are defined as $a_{21,k} = 0.4 b_{1,k}$, where $b_{1,k}$, $k = 1, \ldots, q+1$, are the coefficients of a low-pass FIR filter of order $q = 20$ with cutoff frequency equal to 0.2 Hz. Similarly, the coefficients $a_{31,k}$ are defined as $a_{31,k} = 0.6 b_{2,k}$, where $b_{2,k}$, $k = 1, \ldots, q+1$, are the coefficients of a high-pass FIR filter of order $q = 20$ with cutoff frequency equal to 0.2 Hz.

Starting from the model parameters in Eq. (S42) set as described above, the theoretical spectral profiles of the various PIRD and PDGC measures were computed directly in the frequency domain. For each configuration, one process was selected as target, $Y \in \{S_1, S_2, S_3\}$, while the remaining two processes were collected in the source vector $X = \{S_1, S_2, S_3\} \backslash Y$. The decomposition was therefore performed on the redundancy lattice for $N = 2$ sources shown in Fig. 1a of the main paper. In this case, the four atoms of the lattice directly correspond to the two unique components, the redundant component, and the synergistic component. Thus, the PIRD yielded the spectral components $i^{\mathcal{U}}_{X_1;Y}(\omega)$, $i^{\mathcal{U}}_{X_2;Y}(\omega)$, $i^{\mathcal{R}}_{X;Y}(\omega)$, and $i^{\mathcal{S}}_{X;Y}(\omega)$, while the corresponding PDGC analysis yielded $f^{\mathcal{U}}_{X_1\to Y}(\omega)$, $f^{\mathcal{U}}_{X_2\to Y}(\omega)$, $f^{\mathcal{R}}_{X\to Y}(\omega)$, and $f^{\mathcal{S}}_{X\to Y}(\omega)$. This simulation is implemented by the script `SCRIPT_Simu2.m` of the HOP Matlab toolbox. We applied the two frameworks to the VAR parameters of the simulated process to compare the corresponding spectral decomposition profiles. The resulting spectral MIR and GC, together

with their unique, redundant, and synergistic components, are reported in Fig. S3, with each row corresponding to a different chosen target.

When $Y = S_3$, the spectral profiles of the MIR and GC measures are fully overlapping, with two main peaks around 0.1 Hz and 0.35 Hz, corresponding to the oscillatory components present in the dynamics of the process. This agreement is consistent with the imposed VAR structure, characterized by the absence of directed flows from S_3 to S_2 and S_1, and from S_2 to S_1, i.e., $f_{S_3\to S_2}(\omega) = f_{S_3\to S_1}(\omega) = f_{S_2\to S_1}(\omega) = 0$, as well as by the absence of instantaneous interactions. The analysis of the redundant and synergistic spectral components further reveals a prevalence of redundancy over synergy. Specifically, the synergistic contribution, quantified by $i^S_{X;Y}(\omega)$ and $f^S_{X\to Y}(\omega)$, is mainly confined to the oscillatory activity around 0.1 Hz, consistently with the common-child structure $S_1 \to S_3 \leftarrow S_2$. In contrast, the redundant contribution, quantified by $i^R_{X;Y}(\omega)$ and $f^R_{X\to Y}(\omega)$, is mainly driven by the oscillation around 0.35 Hz, which originates from S_1 and is transmitted toward S_3 through a chain-like interaction structure.

A different situation is observed when $Y = S_2$. In this case, the PIRD framework yields spectral profiles of redundant and synergistic information that are similar to those observed for S_3, with the exception of an additional unique information-rate contribution appearing around 0.35 Hz as a consequence of the direct interaction from S_1 to S_2. Conversely, the PDGC framework provides a different decomposition: since the direct interaction from S_3 to S_2 is absent, i.e., $f_{S_3\to S_2}(\omega) = 0$, the redundant and synergistic spectral GC components vanish, and the total spectral GC $f_{X\to Y}(\omega)$ is entirely driven by the unique GC contribution from S_1 to S_2.

The last case, obtained by selecting $Y = S_1$, represents the most extreme configuration. In this setting, the PIRD framework still detects both redundant and synergistic spectral information-rate contributions, with profiles that remain comparable to those observed for the other targets. In contrast, all PDGC components are equal to zero, since no direct connections from the two sources S_2 and S_3 are directed toward the target S_1.

Overall, these results show that the two frameworks provide consistent descriptions only when the statistical dependencies captured by PIRD correspond to causal interactions directed towards the process that is chosen as the target for the decomposition, an when causal interactions originating from such target are negligible. On the contrary, the two approaches provide different descriptions which respond to the nature of the dynamic interactions quantified by PDGC and PIRD: while PDGC isolates the portion of the interaction structure associated with Granger-causal effects directed towards the assigned target, PIRD also captures statistical dependencies that may arise from causal effects originating in the target, or bidirectional effects. This distinction explains why redundant and synergistic information-rate contributions can still be observed in PIRD even when the corresponding redundant and synergistic GC components vanish, and documents the eligibility of PDGC as a tool to dissect dynamic and directed multivariate interactions in networks of random processes.

REFERENCES

[1] L. Faes, L. Sparacino, G. Mijatovic, Y. Antonacci, L. Ricci, D. Marinazzo, and S. Stramaglia, "Partial information rate decomposition," *Phys. Rev. Lett.*, vol. 135, no. 18, p. 187401, 2025.

[2] L. Faes, G. Mijatovic, R. Pernice, D. Marinazzo, S. Stramaglia, and Y. Antonacci, "Dissecting spectral granger causality through partial information decomposition," 2026. [Online]. Available: https://arxiv.org/abs/2603.07634

[3] L. Sparacino, G. Mijatovic, Y. Antonacci, L. Ricci, D. Marinazzo, S. Stramaglia, and L. Faes, "Decomposing multivariate information rates in networks of random processes," *Phys. Rev. E*, vol. 112, no. 4, p. 044313, 2025.

[4] G. Mijatovic, Y. Antonacci, T. Loncar-Turukalo, L. Minati, and L. Faes, "An information-theoretic framework to measure the dynamic interaction between neural spike trains," *IEEE Trans. Biomed. Eng.*, vol. 68, no. 12, pp. 3471–3481, 2021.

[5] L. Barnett, A. B. Barrett, and A. K. Seth, "Granger causality and transfer entropy are equivalent for gaussian variables," *Phys. Rev. Lett.*, vol. 103, no. 23, p. 238701, 2009.

[6] L. Faes, G. Mijatovic, Y. Antonacci, R. Pernice, C. Barà, L. Sparacino, M. Sammartino, A. Porta, D. Marinazzo, and S. Stramaglia, "A new framework for the time-and frequency-domain assessment of high-order interactions in networks of random processes," *IEEE Trans. Sig. Proc.*, vol. 70, pp. 5766–5777, 2022.

[7] H. Akaike, "A new look at the statistical model identification," *IEEE transactions on automatic control*, vol. 19, no. 6, pp. 716–723, 1974.

[8] A. A. Neath and J. E. Cavanaugh, "The bayesian information criterion: background, derivation, and applications," *WIREs Comput. Stat.*, vol. 4, no. 2, p. 199–203, Feb. 2012. [Online]. Available: https://doi.org/10.1002/wics.199

[9] L. Faes, S. Erla, and G. Nollo, "Measuring connectivity in linear multivariate processes: definitions, interpretation, and practical analysis," *Comp. Math. Methods Med.*, vol. 2012, no. 1, p. 140513, 2012.

[10] L. Barnett and A. K. Seth, "Granger causality for state-space models," *Phys. Rev. E.*, vol. 91, no. 4, p. 040101, 2015.

[11] J. Geweke, "Measurement of linear dependence and feedback between multiple time series," *J. Am. Stat. Ass.*, vol. 77, no. 378, pp. 304–313, 1982.

[12] F. E. Rosas, P. A. Mediano, H. J. Jensen, A. K. Seth, A. B. Barrett, R. L. Carhart-Harris, and D. Bor, "Reconciling emergences: An information-theoretic approach to identify causal emergence in multivariate data," *PLoS Comput. Biol.*, vol. 16, no. 12, p. e1008289, 2020.

[13] Y. Antonacci, C. Bará, L. Sparacino, G. Mijatovic, L. Minati, and L. Faes, "A method for the time-frequency analysis of high-order interactions in non-stationary physiological networks," *Journal of Neural Engineering*, vol. 22, no. 6, p. 066001, 2025.